

CommonRoad: Vehicle Models

(Version 2017a)

Matthias Althoff

Technische Universität München, 85748 Garching, Germany

Abstract

This document presents models in *CommonRoad* for vehicle dynamics ranging from simple to complicated: The simplest model is a point-mass model, while the most complicated one is a multi-body model. All models are presented in state-space form to facilitate their implementation in standard solvers for ordinary differential equations. We further provide parameter sets and a precise initialization of the multi-body model. To be able to compare the results with simpler models, it is presented how the initial states and the parameters of the multi-body model can be transferred to simpler models. Implementation examples in MATLAB and Python are provided in the *CommonRoad* online repository. The repository also provide routines to convert initial states and parameters. Simulation examples demonstrate the advantages of more complicated models.

Contents

1	Introduction	2
2	Point-Mass Model (PM)	2
2.1	State Space Model	3
2.2	Parameters	3
3	Kinematic Single-Track Model (KS)	3
3.1	State Space Model	4
3.2	Parameters	4
4	Single-Track Model (ST)	5
4.1	State Space Model	6
4.2	Parameters	7
5	Multi-Body Model (MB)	7
5.1	State Variables	8
5.2	Auxiliary Variables	9
5.3	Tire Formulas	13
5.4	Vehicle Dynamics	15
5.5	Parameters	18
6	Conversion of Initial States and Parameters	18
6.1	Conversion of Parameters	18
6.2	Conversion of Initial States	20
7	Examples	22
8	Conclusions	23

1 Introduction

This document is part of the *CommonRoad* benchmark repository for motion planning of road vehicles, alongside other documents for possible cost functions and road scenarios. It is assumed in this document that all vehicles have an underlying controller that can realize a commanded acceleration (positive and negative). Especially for adaptive cruise control, numerous works already exist that realize a commanded acceleration, see e.g. [7, 15]. The effects on engine characteristics in terms of fuel consumption can be considered in the cost function as demonstrated in the document on cost functions.

The lateral dynamics, however, cannot be abstracted away to the same extent using controllers. Especially, when constraints such as the danger of roll-over have to be considered in extreme maneuvers [4, 9]. For this reason, our models consider increasingly complicated lateral vehicle dynamics and tire models: point-mass model, kinematic single-track model, single-track model, and a multi-body model. For each model, we (1) present the set of required ordinary differential equations, (2) convert them into state-space form so that common solvers can be used, and (3) provide typical parameters.

In *CommonRoad V1.0*, we provide three types of vehicles:

- a small vehicle (Ford Escort; vehicle ID: 1),
- a medium vehicle (BMW 320i; vehicle ID: 2),
- and a van (VW Vanagon; vehicle ID: 3).

Detailed parameters of these vehicles have been collected from [1, Appendix A] and other vehicle databases that are online available. For each vehicle, we provide the aforementioned models: point-mass model (Sec. 2), kinematic single-track model (Sec. 3), single-track model (Sec. 4), and a multi-body model (Sec. 5). After combining the vehicle identifier with the model type, one obtains the model ID. For instance, KS2 is a kinematic single-track model using the parameters of the BMW 320i. In addition, we describe in Sec. 6 how parameters and initial states can be converted from complicated to simpler models. Finally, in Sec. 7 we provide some numerical results.

2 Point-Mass Model (PM)

The point-mass model is the simplest model that is commonly used for motion planning, see e.g. [5, 16]. This model abstracts the vehicle as a point mass that can be accelerated within bounds. This bound is typically chosen as a circle (Kamm’s circle), which is also the bound chosen in this benchmark suite. Let us introduce \square as the placeholder for a variable and \square_x and \square_y to denote the value of the corresponding variable in x and y direction, respectively. After further introducing position s , acceleration a , and maximum absolute acceleration a_{\max} , the dynamics of the point mass model is

$$\ddot{s}_x = a_x, \quad \ddot{s}_y = a_y, \quad \sqrt{a_x^2 + a_y^2} \leq a_{\max}.$$

The point-mass model ignores that vehicles have a minimum turning circle, which is considered in the kinematic single-track model.

2.1 State Space Model

After introducing the state variables x_i as

$$x_1 = s_x, \quad x_2 = s_y, \quad x_3 = \dot{s}_x, \quad x_4 = \dot{s}_y$$

and the input variables u_i as

$$u_1 = a_x, \quad u_2 = a_y,$$

the system dynamics can be written as the linear system

$$\dot{x} = Ax + Bu, \quad A = \begin{bmatrix} 0 & 0 & 1 & 0 \\ 0 & 0 & 0 & 1 \\ 0 & 0 & 0 & 0 \\ 0 & 0 & 0 & 0 \end{bmatrix}, \quad B = \begin{bmatrix} 0 & 0 \\ 0 & 0 \\ 1 & 0 \\ 0 & 1 \end{bmatrix}.$$

The only constraint in state space form is $\sqrt{u_1^2 + u_2^2} \leq a_{\max}$.

2.2 Parameters

The only parameter of this model is a_{\max} . Since in the first version 1.0, all vehicles use the same tire, we have $a_{\max} = 11.5 \text{ [m/s}^2\text{]}$ (see Tab. 2).

3 Kinematic Single-Track Model (KS)

The kinematic single-track models a road vehicle with only two wheels, where the front and rear wheel pairs are each lumped into one wheel. This simplification is justified since the roll dynamics is not considered (see Fig. 1 and [13, Sec. 2.2]). This also explains the term *single-track model*. The kinematic single-track model further does not consider any tire slip, so that the velocity vector v is always aligned with the link between the front and rear wheel. This corresponds to a slip angle $\beta = 0$, which is depicted in Fig. 1. Similarly to the point-mass model, the kinematic single-track model is used in many works for motion planning, e.g. [11, 12]. A simple example, where the benefit of a kinematic single-track model is evident, is parking: a point-mass model is not sufficient since it would not consider the non-holonomic behavior and in particular the minimum turning radius.

In addition to the variables already introduced for the point-mass model and the already introduced velocity v , we additionally require the velocity of the steering angle v_δ , the steering angle δ , the heading Ψ , and the parameters l_{wb} describing the wheelbase as well as the parameter v_S describing the velocity above which the engine power is not sufficient to cause wheel slip (all variables and the parameter l_{wb} are visualized in Fig. 1). We denote by $\underline{\square}$ the minimum possible value and by $\overline{\square}$ the maximum possible value and by \square_{lat} the value of a variable in lateral direction and by \square_{long} the value in longitudinal direction. The differential equations of the kinematic single-track model as defined in this work are

$$\begin{aligned} \dot{\delta} &= v_\delta, \\ \dot{\Psi} &= \frac{v}{l_{wb}} \tan(\delta), \\ \dot{v} &= a_{\text{long}}, \\ \dot{s}_x &= v \cos(\Psi), \\ \dot{s}_y &= v \sin(\Psi), \end{aligned} \tag{1}$$

where

$$v_\delta \in [-\bar{v}_\delta, \bar{v}_\delta], \quad \delta \in [-\bar{\delta}, \bar{\delta}], \quad v \in [\underline{v}, \bar{v}], \quad (2)$$

$$a_{\text{long}} \in [-a_{\text{max}}, \bar{a}], \quad \bar{a} = \begin{cases} \bar{a} = a_{\text{max}} \frac{v_S}{v} & \text{for } v > v_S, \\ \bar{a} = a_{\text{max}} & \text{otherwise,} \end{cases} \quad (3)$$

$$\sqrt{a_{\text{long}}^2 + (v \dot{\Psi})^2} \leq a_{\text{max}} \quad (a_{\text{lat}} = v \dot{\Psi}) \quad (4)$$

Please note that kinematic single-track models slightly differ in publications, depending on whether one considers that (1) the steering angle or the steering velocity is an input or (2) the vehicle velocity or the vehicle acceleration is an input. For instance, in [11, eq. (8)], the vehicle velocity and the steering velocity are inputs. We would also like to mention, that other works do not provide all the constraints of our model (which can be easily removed, but a removal should be stated since this simplifies motion planning).

Constraint (6) models that vehicles have limited engine power and braking power as detailed in [2, Sec. III.B]. As in the point-mass model, constraint (4) models Kamm's circle.

3.1 State Space Model

To write the kinematic single-track model in state-space form, we introduce the following state variables:

$$x_1 = s_x, \quad x_2 = s_y, \quad x_3 = \delta, \quad x_4 = v, \quad x_5 = \Psi.$$

The input variables are

$$u_1 = v_\delta, \quad u_2 = a_{\text{long}}. \quad (5)$$

Inserting the state and input variables into (1) results in

$$\begin{aligned} \dot{x}_1 &= x_4 \cos(x_3), \\ \dot{x}_2 &= x_4 \sin(x_3), \\ \dot{x}_3 &= u_1, \\ \dot{x}_4 &= u_2, \\ \dot{x}_5 &= \frac{x_4}{l_{wb}} \tan(x_3). \end{aligned}$$

Using state variables, the constraints become

$$\begin{aligned} u_1 &\in [\underline{v}_\delta, \bar{v}_\delta], \quad x_3 \in [\underline{\delta}, \bar{\delta}], \quad x_4 \in [\underline{v}, \bar{v}], \\ u_2 &\in [-a_{\text{max}}, \bar{a}], \quad \bar{a} = \begin{cases} \bar{a} = a_{\text{max}} \frac{v_S}{x_4} & \text{for } x_4 > v_S, \\ \bar{a} = a_{\text{max}} & \text{otherwise,} \end{cases} \\ \sqrt{u_2^2 + (x_4 \dot{x}_5)^2} &\leq a_{\text{max}}. \end{aligned} \quad (6)$$

3.2 Parameters

The parameters of this model are listed in Tab. 1 and the constraint parameters are presented in Tab. 2.

Table 1: Vehicle Parameters for the kinematic single-track model (values have been obtained according to Sec. 6.1).

vehicle parameter			vehicle identifier		
name	symbol	unit	1	2	3
vehicle length	l	[m]	4.298	4.508	4.569
vehicle width	w	[m]	1.674	1.610	1.844
wheelbase	l_{wb}	[m]	2.391	2.578	2.471

Table 2: Constraint Parameters (obtained from own research of information from the web).

vehicle parameter			vehicle identifier		
name	symbol	unit	1	2	3
minimum steering angle	$\underline{\delta}$	[rad]	-0.910	-1.066	-1.023
maximum steering angle	$\bar{\delta}$	[rad]	0.910	1.066	1.023
minimum steering velocity	\underline{v}_{δ}	[rad/s]	-0.4	-0.4	-0.4
maximum steering velocity	\bar{v}_{δ}	[rad/s]	0.4	0.4	0.4
min. velocity (also depending on traffic rules)	\underline{v}	[m/s]	0	0	0
max. velocity (also depending on traffic rules)	\bar{v}	[m/s]	45.8	50.8	41.7
switching velocity	v_S	[m/s]	4.755	7.319	4.824
maximum acceleration	a_{\max}	[m/s ²]	11.5	11.5	11.5

4 Single-Track Model (ST)

Since the kinematic single-track model does not consider tire slip, important effects such as understeer or oversteer are not considered [13, Sec. 2.3]. However, when the vehicle is not driving close to its physical capabilities, those effects are not dominant. The extension is the well-known single-track model, which is also known as the bicycle model. Works that perform planning of evasive maneuvers closer to physical limits require the single-track model, see e.g. [6, 14]. We additionally consider the load transfer of the vehicle due to longitudinal acceleration a_{long} (neglecting suspension dynamics), such that the vertical forces on the front and rear axis $F_{z,f}$ and $F_{z,r}$ become

$$F_{z,f} = \frac{mgl_r - ma_{\text{long}}h_{cg}}{l_r + l_f}, \quad F_{z,r} = \frac{mgl_f + ma_{\text{long}}h_{cg}}{l_r + l_f},$$

with parameters from Tab. 3. These forces are inserted into the derivation of the equations for the slip angle (at the center of gravity) β and the yaw rate $\dot{\Psi}$ [13, Sec. 2.3]. Using the previously introduced variables and the parameters in Tab. 3, the single-track model as defined in this

work is

$$\begin{aligned}
\dot{\delta} &= v_{\delta}, \\
\dot{\beta} &= \frac{\mu}{v(l_r + l_f)} \left(C_{S,f}(gl_r - a_{\text{long}}h_{cg})\delta - (C_{S,r}(gl_f + a_{\text{long}}h_{cg}) + C_{S,f}(gl_r - a_{\text{long}}h_{cg}))\beta \right. \\
&\quad \left. + (C_{S,r}(gl_f + a_{\text{long}}h_{cg})l_r - C_{S,f}(gl_r - a_{\text{long}}h_{cg})l_f)\frac{\dot{\Psi}}{v} \right) - \dot{\Psi}, \\
\ddot{\Psi} &= \frac{\mu m}{I_z(l_r + l_f)} \left(l_f C_{S,f}(gl_r - a_{\text{long}}h_{cg})\delta \right. \\
&\quad \left. + (l_r C_{S,r}(gl_f + a_{\text{long}}h_{cg}) - l_f C_{S,f}(gl_r - a_{\text{long}}h_{cg}))\beta \right. \\
&\quad \left. - (l_f^2 C_{S,f}(gl_r - a_{\text{long}}h_{cg}) + l_r^2 C_{S,r}(gl_f + a_{\text{long}}h_{cg}))\frac{\dot{\Psi}}{v} \right), \\
\dot{v} &= a_{\text{long}}, \\
\dot{s}_x &= v \cos(\beta + \Psi), \\
\dot{s}_y &= v \sin(\beta + \Psi),
\end{aligned} \tag{7}$$

under consideration of (2)-(4). Please note that in contrast to this work, other works often only consider constant velocity when referring to a single-track model (see e.g. [13, Sec. 2.3]). Also, the weight transfer between the front and rear axle is often neglected in single-track models (see e.g. [6]). Note that we do not use the cornering stiffness C , as is typically done for single-track models, but separate the effect of the friction coefficient μ , the cornering stiffness coefficient C_S , and the vertical force F_z , such that $C_i = \mu C_{S,i} F_{z,i}$ and $i = \{f, r\}$ for the front and rear axle. This separation is done because the friction coefficient is the most dominant parameter modeling the influence of weather.

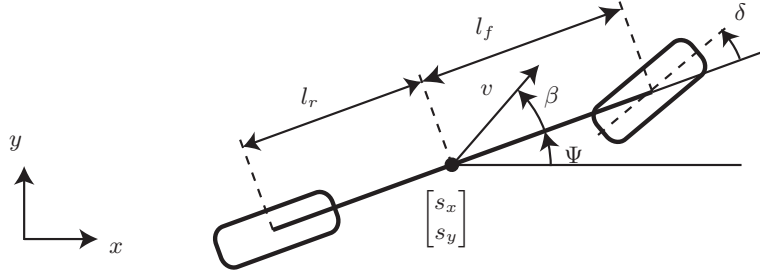


Figure 1: Single-track model.

4.1 State Space Model

The single-track model requires a few more state variables compared to the kinematic single-track model. In order to share the constraint functions in (??), we keep the numbering of state variable shared with the kinematic single-track model:

$$x_1 = s_x, \quad x_2 = s_y, \quad x_3 = \delta, \quad x_4 = v, \quad x_5 = \Psi, \quad x_6 = \dot{\Psi}, \quad x_7 = \beta.$$

The input variables are identical to (5). Inserting the state and input variables into (7) results in

$$\begin{aligned}
\dot{x}_1 &= x_4 \cos(x_5 + x_7), \\
\dot{x}_2 &= x_4 \sin(x_5 + x_7), \\
\dot{x}_3 &= u_1, \\
\dot{x}_4 &= u_2, \\
\dot{x}_5 &= x_6, \\
\dot{x}_6 &= \frac{\mu m}{I_z(l_r + l_f)} \left(l_f C_{S,f}(gl_r - u_2 h_{cg}) x_3 + (l_r C_{S,r}(gl_f + u_2 h_{cg}) - l_f C_{S,f}(gl_r - u_2 h_{cg})) x_7 \right. \\
&\quad \left. - (l_f^2 C_{S,f}(gl_r - u_2 h_{cg}) + l_r^2 C_{S,r}(gl_f + u_2 h_{cg})) \frac{x_6}{x_4} \right), \\
\dot{x}_7 &= \frac{\mu}{x_4(l_r + l_f)} \left(C_{S,f}(gl_r - u_2 h_{cg}) x_3 - (C_{S,r}(gl_f + u_2 h_{cg}) + C_{S,f}(gl_r - u_2 h_{cg})) x_7 \right. \\
&\quad \left. + (C_{S,r}(gl_f + u_2 h_{cg}) l_r - C_{S,f}(gl_r - u_2 h_{cg}) l_f) \frac{x_6}{x_4} \right) - x_6.
\end{aligned} \tag{8}$$

Due to the special choice of state variables, the constraints are identical to (??).

4.2 Parameters

The parameters of the single-track model are listed in Tab. 3 and the constraint parameters are identical to Tab. 2.

Table 3: Vehicle Parameters for the single-track model (values have been obtained according to Sec. 6.1).

vehicle parameter			vehicle identifier		
name	symbol	unit	1	2	3
vehicle length	l	[m]	4.298	4.508	4.569
vehicle width	w	[m]	1.674	1.610	1.844
total vehicle mass	m	10^3 [kg]	1.225	1.093	1.478
moment of inertia for entire mass about z axis	I_z	10^3 [kg m ²]	1.538	1.791	2.473
distance from center of gravity to front axle	l_f	[m]	0.883	1.156	1.150
distance from center of gravity to rear axle	l_r	[m]	1.508	1.422	1.321
center of gravity height of total mass	h_{cg}	[m]	0.557	0.574	0.747
cornering stiffness coefficient (front)	$C_{S,f}$	[1/rad]	20.89	20.89	20.89
friction coefficient	μ	[-]	1.048	1.048	1.048

5 Multi-Body Model (MB)

Although the previously introduced single-track model considers already many important effects of vehicle dynamics, it does not consider the vertical load of all 4 wheels due to roll, pitch, and yaw, their individual spin and slip, and nonlinear tire dynamics. An example where a multi-body model is used for motion planning of a road vehicle is [3]. Although many commercial multi-body models for vehicle dynamics exist¹, those models are proprietary and thus not appropriate for a benchmark that requires public accessibility. Our multi-body model is taken out of [1, Appendix A], which is one of few detailed and accessible multi-body dynamics descriptions. For easy use,

¹www.carsim.com, www.thesis-dynaware.com, www.mscsoftware.com

we have translated the equations in [1, Appendix A] into a state space model, which is more suitable for implementation in ordinary-differential-equation solvers. A MATLAB and a Python implementation can be found in [jrepository here](#).

The multi-body dynamics is described by 3 masses: The unsprung mass and the sprung mass of the front and rear axles. The forces between these masses are described by the dynamics of the suspension and the tire model. We consider all suspension forces in [1, Appendix A] originating from springs, dampers, and anti-roll bars. We do not consider flexibilities in the steering system, bump stops, and squat/lift forces caused by the suspension geometry. All considered vehicles have an independent suspension so that we do not show the equations for solid axes. For the tire dynamics we use the PAC2002 Magic-Formula tire model, which is widely used in industry [8]. The combined lateral and longitudinal tire forces are computed from the slip angle, the camber angle, and the vertical tire force described in [1, Appendix A]. The tire parameters for all 4 wheels are taken from the example of a PAC2002 tire property file in [8]. Rewriting all equations as a state space model yields 29 state variables. All state variables, including their initial values, are listed in Tab. 6, where the pairs LF , RF , LR , RR indicate left/right and front/rear.

Compared to [1, Appendix A] the equations are presented in an order so that equations depend on previously computed results, making it possible to directly implement them; see our MATLAB and Python implementation in [jrepository here](#).

5.1 State Variables

We group the state variables into *vehicle body*, *front axle*, *rear axle*, *wheels*, and *auxiliary*.

Vehicle body

- $x_1 = s_x$ (x-position in a global coordinate system),
- $x_2 = s_y$ (y-position in a global coordinate system),
- $x_3 = \delta$ (steering angle of front wheels),
- $x_4 = v_x$ (velocity in longitudinal direction in the vehicle-fixed coordinate system),
- $x_5 = \Psi$ (yaw angle),
- $x_6 = \dot{\Psi}$ (yaw rate),
- $x_7 = \Phi_S$ (roll angle),
- $x_8 = \dot{\Phi}_S$ (roll rate),
- $x_9 = \Theta_S$ (pitch angle),
- $x_{10} = \dot{\Theta}_S$ (pitch rate),
- $x_{11} = v_y$ (velocity in lateral direction in the vehicle-fixed coordinate system),
- $x_{12} = s_z$ (z-position (height) from ground),
- $x_{13} = v_z$ (velocity in vertical direction perpendicular to road plane),

Front axle

$$\begin{aligned}
x_{14} &= \Phi_{UF} \quad (\text{roll angle front}), \\
x_{15} &= \dot{\Phi}_{UF} \quad (\text{roll rate front}), \\
x_{16} &= v_{y,UF} \quad (\text{velocity in y-direction front}), \\
x_{17} &= s_{z,UF} \quad (\text{z-position front}), \\
x_{18} &= v_{z,UF} \quad (\text{velocity in z-direction front}),
\end{aligned}$$

Rear axle

$$\begin{aligned}
x_{19} &= \Phi_{UR} \quad (\text{roll angle rear}), \\
x_{20} &= \dot{\Phi}_{UR} \quad (\text{roll rate rear}), \\
x_{21} &= v_{y,UR} \quad (\text{velocity in y-direction rear}), \\
x_{22} &= s_{z,UR} \quad (\text{z-position rear}), \\
x_{23} &= v_{z,UR} \quad (\text{velocity in z-direction rear}),
\end{aligned}$$

Wheels

$$\begin{aligned}
x_{24} &= \omega_{LF} \quad (\text{left front wheel angular velocity}), \\
x_{25} &= \omega_{RF} \quad (\text{right front wheel angular velocity}), \\
x_{26} &= \omega_{LR} \quad (\text{left rear wheel angular velocity}), \\
x_{27} &= \omega_{RR} \quad (\text{right rear wheel angular velocity})
\end{aligned}$$

Auxiliary

$$\begin{aligned}
x_{28} &= \delta_{y,f}, \\
x_{29} &= \delta_{y,r}
\end{aligned}$$

5.2 Auxiliary Variables

Slip angle and velocity at center of gravity These equations are derived by the author:

$$\begin{aligned}
\beta &= \arctan \left(\frac{x_{11}}{x_4} \right) \\
v_{CG} &= \sqrt{x_4^2 + x_{11}^2}
\end{aligned}$$

Vertical tire forces These equations are obtained from [1, eq. A48-A51]:

$$\begin{aligned}
F_{z,LF} &= (x_{17} + R_w(\cos(x_{14}) - 1) - \frac{1}{2}T_f \sin(x_{14}))K_{zt} \\
F_{z,RF} &= (x_{17} + R_w(\cos(x_{14}) - 1) + \frac{1}{2}T_f \sin(x_{14}))K_{zt} \\
F_{z,LR} &= (x_{22} + R_w(\cos(x_{19}) - 1) - \frac{1}{2}T_r \sin(x_{19}))K_{zt} \\
F_{z,RR} &= (x_{22} + R_w(\cos(x_{19}) - 1) + \frac{1}{2}T_r \sin(x_{19}))K_{zt}
\end{aligned}$$

Individual tire velocities These equations are derived from [1, eq. A56-A59] assuming that the rear wheels cannot be steered and by using $x_4 \tan(\beta) = x_{11}$ from [1, p. A45]:

$$\begin{aligned} u_{w,LF} &= (x_4 + \frac{1}{2}T_f x_6) \cos(x_3) + (x_{11} + l_f x_6) \sin(x_3) \\ u_{w,RF} &= (x_4 - \frac{1}{2}T_f x_6) \cos(x_3) + (x_{11} + l_f x_6) \sin(x_3) \\ u_{w,LR} &= x_4 + \frac{1}{2}T_r x_6 \\ u_{w,RR} &= x_4 - \frac{1}{2}T_r x_6 \end{aligned}$$

Longitudinal slip These equations are taken from [1, eq. A60]:

$$\begin{aligned} s_{LF} &= 1 - \frac{R_w x_{24}}{u_{w,LF}} \\ s_{RF} &= 1 - \frac{R_w x_{25}}{u_{w,RF}} \\ s_{LR} &= 1 - \frac{R_w x_{26}}{u_{w,LR}} \\ s_{RR} &= 1 - \frac{R_w x_{27}}{u_{w,RR}} \end{aligned}$$

Lateral slip angles These equations are taken from [1, eq. A42-A45] assuming that the rear wheels cannot be steered:

$$\begin{aligned} \alpha_{LF} &= \arctan \left(\frac{x_{11} + l_f x_6 - x_{15}(R_w - x_{17})}{x_4 + \frac{1}{2}T_f x_6} \right) - x_3 \\ \alpha_{RF} &= \arctan \left(\frac{x_{11} + l_f x_6 - x_{15}(R_w - x_{17})}{x_4 - \frac{1}{2}T_f x_6} \right) - x_3 \\ \alpha_{LR} &= \arctan \left(\frac{x_{11} - l_r x_6 - x_{20}(R_w - x_{22})}{x_4 + \frac{1}{2}T_r x_6} \right) \\ \alpha_{RR} &= \arctan \left(\frac{x_{11} - l_r x_6 - x_{20}(R_w - x_{22})}{x_4 - \frac{1}{2}T_r x_6} \right) \end{aligned}$$

Auxiliary suspension movement These equations are taken from [1, eq. A23a-A26a] and [1, eq. A23b-A26b]:

$$\begin{aligned} z_{S,LF} &= \frac{h_s - R_w + x_{17} - x_{12}}{\cos(x_7)} - h_s + R_w + l_f x_9 + \frac{1}{2}(x_7 - x_{14})T_f \\ z_{S,RF} &= \frac{h_s - R_w + x_{17} - x_{12}}{\cos(x_7)} - h_s + R_w + l_f x_9 - \frac{1}{2}(x_7 - x_{14})T_f \\ z_{S,LR} &= \frac{h_s - R_w + x_{22} - x_{12}}{\cos(x_7)} - h_s + R_w - l_r x_9 + \frac{1}{2}(x_7 - x_{19})T_r \\ z_{S,RR} &= \frac{h_s - R_w + x_{22} - x_{12}}{\cos(x_7)} - h_s + R_w - l_r x_9 - \frac{1}{2}(x_7 - x_{19})T_r \end{aligned}$$

$$\begin{aligned}
\dot{z}_{S,LF} &= x_{18} - x_{13} + l_f x_{10} + \frac{1}{2}(x_8 - x_{15})T_f \\
\dot{z}_{S,RF} &= x_{18} - x_{13} + l_f x_{10} - \frac{1}{2}(x_8 - x_{15})T_f \\
\dot{z}_{S,LR} &= x_{23} - x_{13} - l_r x_{10} + \frac{1}{2}(x_8 - x_{20})T_r \\
\dot{z}_{S,RR} &= x_{23} - x_{13} - l_r x_{10} - \frac{1}{2}(x_8 - x_{20})T_r \text{ ('-' changed to '+' compared to [1, eq. A26b])}
\end{aligned}$$

Camber angles These equations are taken from [1, eq. A27-A30]:

$$\begin{aligned}
\gamma_{LF} &= x_7 + D_f z_{S,LF} + E_f (z_{S,LF})^2 \\
\gamma_{RF} &= x_7 - D_f z_{S,RF} - E_f (z_{S,RF})^2 \\
\gamma_{LR} &= x_7 + D_r z_{S,LR} + E_r (z_{S,LR})^2 \\
\gamma_{RR} &= x_7 - D_r z_{S,RR} - E_r (z_{S,RR})^2
\end{aligned}$$

Auxiliary movements/forces for compliant joint equations These equations are taken from [1, eq. A61-A68]:

$$\begin{aligned}
\Delta z_F &= h_s - R_w + x_{17} - x_{12} \\
\Delta z_R &= h_s - R_w + x_{22} - x_{12}
\end{aligned}$$

$$\begin{aligned}
\Delta \phi_F &= x_7 - x_{14} \\
\Delta \phi_R &= x_7 - x_{19}
\end{aligned}$$

$$\begin{aligned}
\Delta \dot{\phi}_F &= x_8 - x_{15} \\
\Delta \dot{\phi}_R &= x_8 - x_{20}
\end{aligned}$$

$$\begin{aligned}
\Delta \dot{z}_F &= x_{18} - x_{13} \\
\Delta \dot{z}_R &= x_{23} - x_{13}
\end{aligned}$$

$$\begin{aligned}
\Delta \dot{y}_F &= x_{11} + l_f x_6 - x_{16} \\
\Delta \dot{y}_R &= x_{11} - l_r x_6 - x_{21}
\end{aligned}$$

$$\begin{aligned}
\Delta_F &= \Delta z_F \sin(x_7) - x_{28} \cos(x_7) - (h_{RAF} - R_w) \sin(\Delta \phi_F) \\
\Delta_R &= \Delta z_R \sin(x_7) - x_{29} \cos(x_7) - (h_{RAR} - R_w) \sin(\Delta \phi_R)
\end{aligned}$$

$$\begin{aligned}
\dot{\Delta}_F &= (\Delta z_F \cos(x_7) + x_{28} \sin(x_7))x_8 + \Delta \dot{z}_F \sin(x_7) - \Delta \dot{y}_F \cos(x_7) - (h_{RAF} - R_w) \cos(\Delta \phi_F) \Delta \dot{\phi}_F \\
\dot{\Delta}_R &= (\Delta z_R \cos(x_7) + x_{29} \sin(x_7))x_8 + \Delta \dot{z}_R \sin(x_7) - \Delta \dot{y}_R \cos(x_7) - (h_{RAR} - R_w) \cos(\Delta \phi_R) \Delta \dot{\phi}_R
\end{aligned}$$

$$\begin{aligned}
F_{RAF} &= \Delta_F K_{RAS} + \dot{\Delta}_F K_{RAD} \\
F_{RAR} &= \Delta_R K_{RAS} + \dot{\Delta}_R K_{RAD}
\end{aligned}$$

Auxiliary suspension forces (bump stop neglected; squat/lift forces neglected) These equations are taken from [1, eq. A23-A26] and [1, p. A51]:

$$\begin{aligned}
F_{S,LF} &= \frac{m_s g l_r}{2(l_f + l_r)} - z_{S,LF} K_{S,F} - \dot{z}_{S,LF} K_{SD,F} + \frac{(x_7 - x_{14})K_{TS,F}}{T_f} \\
F_{S,RF} &= \frac{m_s g l_r}{2(l_f + l_r)} - z_{S,RF} K_{S,F} - \dot{z}_{S,RF} K_{SD,F} - \frac{(x_7 - x_{14})K_{TS,F}}{T_f} \\
F_{S,LR} &= \frac{m_s g l_f}{2(l_f + l_r)} - z_{S,LR} K_{S,R} - \dot{z}_{S,LR} K_{SD,R} + \frac{(x_7 - x_{19})K_{TS,R}}{T_r} \\
F_{S,RR} &= \frac{m_s g l_f}{2(l_f + l_r)} - z_{S,RR} K_{S,R} - \dot{z}_{S,RR} K_{SD,R} - \frac{(x_7 - x_{19})K_{TS,R}}{T_r}
\end{aligned}$$

Auxiliary variables sprung mass These equations are taken from [1, eq. A7-A12]:

$$\begin{aligned}
\sum X &= F_{x,LR} + F_{x,RR} + (F_{x,LF} + F_{x,RF}) \cos(x_3) - (F_{y,LF} + F_{y,RF}) \sin(x_3) \\
\sum N &= (F_{y,LF} + F_{y,RF}) l_f \cos(x_3) + (F_{x,LF} + F_{x,RF}) l_f \sin(x_3) \\
&\quad + (F_{y,RF} - F_{y,LF}) \frac{1}{2} T_f \sin(x_3) + (F_{x,LF} - F_{x,RF}) \frac{1}{2} T_f \cos(x_3) \\
&\quad + (F_{x,LR} - F_{x,RR}) \frac{1}{2} T_r - (F_{y,LR} + F_{y,RR}) l_r \\
\sum Y_s &= (F_{RAF} + F_{RAR}) \cos(x_7) + (F_{S,LF} + F_{S,LR} + F_{S,RF} + F_{S,RR}) \sin(x_7) \\
\sum L &= \frac{1}{2} F_{S,LF} T_f + \frac{1}{2} F_{S,LR} T_r - \frac{1}{2} F_{S,RF} T_f - \frac{1}{2} F_{S,RR} T_r \\
&\quad - \frac{F_{RAF}}{\cos(x_7)} (h_s - x_{12} - R_w + x_{17} - (h_{RAF} - R_w) \cos(x_{14})) \\
&\quad - \frac{F_{RAR}}{\cos(x_7)} (h_s - x_{12} - R_w + x_{22} - (h_{RAR} - R_w) \cos(x_{19})) \\
\sum Z_s &= (F_{S,LF} + F_{S,LR} + F_{S,RF} + F_{S,RR}) \cos(x_7) - (F_{RAF} + F_{RAR}) \sin(x_7) \\
\sum M_s &= l_f (F_{S,LF} + F_{S,RF}) - l_r (F_{S,LR} + F_{S,RR}) + ((F_{x,LF} + F_{x,RF}) \cos(x_3) \\
&\quad - (F_{y,LF} + F_{y,RF}) \sin(x_3) + F_{x,LR} + F_{x,RR}) (h_s - x_{12})
\end{aligned}$$

Auxiliary variables unsprung mass These equations are taken from [1, eq. A20-A22] assuming that only the front wheels can be steered:

$$\begin{aligned}
\sum L_{uf} &= \frac{1}{2} F_{S,RF} T_f - \frac{1}{2} F_{S,LF} T_f - F_{RAF} (h_{RAF} - R_w) \\
&\quad + F_{z,LF} (R_w \sin(x_{14}) + \frac{1}{2} T_f \cos(x_{14}) - K_{LT} F_{y,LF}) \\
&\quad - F_{z,RF} (-R_w \sin(x_{14}) + \frac{1}{2} T_f \cos(x_{14}) + K_{LT} F_{y,RF}) \\
&\quad - ((F_{y,LF} + F_{y,RF}) \cos(x_3) + (F_{x,LF} + F_{x,RF}) \sin(x_3)) (R_w - x_{17}) \\
\sum L_{ur} &= \frac{1}{2} F_{S,RR} T_r - \frac{1}{2} F_{S,LR} T_r - F_{RAR} (h_{RAR} - R_w) \\
&\quad + F_{z,LR} (R_w \sin(x_{19}) + \frac{1}{2} T_r \cos(x_{19}) - K_{LT} F_{y,LR}) \\
&\quad - F_{z,RR} (-R_w \sin(x_{19}) + \frac{1}{2} T_r \cos(x_{19}) + K_{LT} F_{y,RR}) \\
&\quad - (F_{y,LR} + F_{y,RR}) (R_w - x_{22}) \\
\sum Z_{uf} &= F_{z,LF} + F_{z,RF} + F_{RAF} \sin(x_7) - (F_{S,LF} + F_{S,RF}) \cos(x_7) \\
\sum Z_{ur} &= F_{z,LR} + F_{z,RR} + F_{RAR} \sin(x_7) - (F_{S,LR} + F_{S,RR}) \cos(x_7) \\
\sum Y_{uf} &= (F_{y,LF} + F_{y,RF}) \cos(x_3) + (F_{x,LF} + F_{x,RF}) \sin(x_3) \\
&\quad - F_{RAF} \cos(x_7) - (F_{S,LF} + F_{S,RF}) \sin(x_7) \\
\sum Y_{ur} &= (F_{y,LR} + F_{y,RR}) \\
&\quad - F_{RAR} \cos(x_7) - (F_{S,LR} + F_{S,RR}) \sin(x_7)
\end{aligned}$$

5.3 Tire Formulas

We are using the Pacejka 2002 tire model [10], which is one of the most popular tire models. The exact parameters for a realistic tire are taken out of [8]. For our particular model, we make the following assumptions:

- Turn slip is neglected, so that $\forall i : \xi_i = 1$;
- Effect of load increment is neglected so that $df_z = 0$ (see [8, PAC2002, eq. 16]);
- All scaling factors are set as $\forall i : \lambda_i = 1$.

Longitudinal tire forces using the magic formula for pure slip $\forall i \in \{LF, RF, LR, RR\}$:

$$\begin{aligned}
S_{Hx} &= p_{Hx1} && \text{(see [8, PAC2002, eq. 27])} \\
S_{Vx,i} &= F_{z,i} p_{Vx1} && \text{(see [8, PAC2002, eq. 28])} \\
\kappa_i &= -s_i && \text{(coord. trans. [1] } \rightarrow \text{ [8])} \\
\kappa_{x,i} &= \kappa_i + S_{Hx} && \text{(see [8, PAC2002, eq. 19])} \\
\mu_{x,i} &= p_{Dx1} (1 - p_{Dx3} \gamma_i^2) && \text{(see [8, PAC2002, eq. 23])} \\
C_x &= p_{Cx1} && \text{(see [8, PAC2002, eq. 21])} \\
D_{x,i} &= \mu_x F_{z,i} && \text{(see [8, PAC2002, eq. 22])} \\
E_x &= p_{Ex1} && \text{(see [8, PAC2002, eq. 24])} \\
K_{x,i} &= F_{z,i} p_{Kx1} && \text{(see [8, PAC2002, eq. 25])} \\
B_{x,i} &= \frac{K_{x,i}}{C_x D_{x,i}} && \text{(see [8, PAC2002, eq. 26])} \\
F_{x0,i} &= D_{x,i} \sin(C_x \arctan(B_{x,i} \kappa_{x,i} - E_x(B_{x,i} \kappa_{x,i} \\
&\quad - \arctan(B_{x,i} \kappa_{x,i}))) + S_{Vx,i} && \text{(see [8, PAC2002, eq. 18])}
\end{aligned}$$

Lateral tire forces using the magic formula for pure slip $\forall i \in \{LF, RF, LR, RR\}$:

$$\begin{aligned}
S_{Hy,i} &= \text{sgn}(\gamma_i)(p_{Hy1} + p_{Hy3} \text{abs}(\gamma_i)) && \text{(see [8, PAC2002, eq. 40])} \\
S_{Vy,i} &= \text{sgn}(\gamma_i) F_{z,i} (p_{Vy1} + p_{Vy3} \text{abs}(\gamma_i)) && \text{(see [8, PAC2002, eq. 41])} \\
\alpha_{y,i} &= \alpha_i + S_{Hy,i} && \text{(see [8, PAC2002, eq. 31])} \\
\mu_{y,i} &= p_{Dy1} (1 - p_{Dy3} \gamma_i^2) && \text{(see [8, PAC2002, eq. 35])} \\
C_y &= p_{Cy1} && \text{(see [8, PAC2002, eq. 33])} \\
D_{y,i} &= \mu_{y,i} F_{z,i} && \text{(see [8, PAC2002, eq. 34])} \\
E_y &= p_{Ey1} && \text{(see [8, PAC2002, eq. 36])} \\
K_{y,i} &= F_{z,i} p_{Ky1} \quad (\text{simplified } K_{y0} \text{ to } p_{Ky1} F_{z,i}) && \text{(see [8, PAC2002, eq. 38])} \\
B_{y,i} &= \frac{K_{y,i}}{C_y D_{y,i}} && \text{(see [8, PAC2002, eq. 39])} \\
F_{y0,i} &= D_{y,i} \sin(C_y \arctan(B_{y,i} \alpha_{y,i} - E_y(B_{y,i} \alpha_{y,i} \\
&\quad - \arctan(B_{y,i} \alpha_{y,i}))) + S_{Vy,i} && \text{(see [8, PAC2002, eq. 30])} \quad (9)
\end{aligned}$$

Longitudinal tire forces for combined slip $\forall i \in \{LF, RF, LR, RR\}$:

$$\begin{aligned}
S_{Hx\alpha} &= r_{Hx1} && \text{(see [8, PAC2002, eq. 65])} \\
\alpha_{s,i} &= \alpha_i + S_{Hx\alpha} && \text{(see [8, PAC2002, eq. 60])} \\
B_{x\alpha,i} &= r_{Bx1} \cos(\arctan(r_{Bx2} \kappa_i)) && \text{(see [8, PAC2002, eq. 61])} \\
C_{x\alpha} &= r_{Cx1} && \text{(see [8, PAC2002, eq. 62])} \\
E_{x\alpha} &= r_{Ex1} && \text{(see [8, PAC2002, eq. 64])} \\
D_{x\alpha,i} &= F_{x0,i} / \cos \left(C_{x\alpha} \arctan \left(B_{x\alpha,i} S_{Hx\alpha} - E_{x\alpha} (B_{x\alpha,i} S_{Hx\alpha} \right. \right. \\
&\quad \left. \left. - \arctan(B_{x\alpha,i} S_{Hx\alpha})) \right) \right) && \text{(see [8, PAC2002, eq. 63])} \\
F_{x,i} &= D_{x\alpha,i} \cos(C_{x\alpha} \arctan(B_{x\alpha,i} \alpha_{s,i} - E_{x\alpha} (B_{x\alpha,i} \alpha_{s,i} \\
&\quad - \arctan(B_{x\alpha,i} \alpha_{s,i})))) && \text{(see [8, PAC2002, eq. 59])}
\end{aligned}$$

Lateral tire forces for combined slip $\forall i \in \{LF, RF, LR, RR\}$:

$$\begin{aligned}
S_{Hy\kappa} &= r_{Hy1} && \text{(see [8, PAC2002, eq. 74])} \\
\kappa_{s,i} &= \kappa_i + S_{Hy\kappa} && \text{(see [8, PAC2002, eq. 69])} \\
B_{y\kappa,i} &= r_{By1} \cos(\arctan(r_{By2} (\alpha_i - r_{By3}))) && \text{(see [8, PAC2002, eq. 70])} \\
C_{y\kappa} &= r_{Cy1} && \text{(see [8, PAC2002, eq. 71])} \\
E_{y\kappa} &= r_{Ey1} && \text{(see [8, PAC2002, eq. 73])} \\
D_{y\kappa} &= F_{y0,i} / \cos \left(C_{y\kappa} \arctan \left(B_{y\kappa,i} S_{Hy\kappa} - E_{y\kappa} (B_{y\kappa,i} S_{Hy\kappa} \right. \right. \\
&\quad \left. \left. - \arctan(B_{y\kappa,i} S_{Hy\kappa})) \right) \right) && \text{(see [8, PAC2002, eq. 72])} \\
D_{vy\kappa,i} &= \mu_{y,i} F_{z,i} (r_{Vy1} + r_{Vy3} \gamma_i) \cos(\arctan(r_{Vy4} \alpha_i)) && \text{(see [8, PAC2002, eq. 76])} \\
S_{vy\kappa,i} &= D_{vy\kappa,i} \sin(r_{Vy5} \arctan(r_{Vy6} \kappa_i)) && \text{(see [8, PAC2002, eq. 75])} \\
F_{y,i} &= D_{y\kappa} \cos(C_{y\kappa} \arctan(B_{y\kappa,i} \kappa_{s,i} - E_{y\kappa} (B_{y\kappa,i} \kappa_{s,i} \\
&\quad - \arctan(B_{y\kappa,i} \kappa_{s,i})))) + S_{Vy\kappa} && \text{(see [8, PAC2002, eq. 68])}
\end{aligned}$$

5.4 Vehicle Dynamics

Based on the auxiliary variables from Sec. 5.2 and the tire forces from Sec. 5.3, we compute the right hand side of the vehicle dynamics $\dot{x} = f(x, u)$ in this subsection:

Dynamics common with single-track model

$$\begin{aligned}
\dot{x}_1 &= v_{CG} \cos(\beta + x_5) && \text{(from (7))} \\
\dot{x}_2 &= v_{CG} \sin(\beta + x_5) && \text{(from (7))} \\
\dot{x}_3 &= u_1 && \text{(trivial)} \\
\dot{x}_4 &= \frac{1}{m} \sum X + x_6 x_{11} && \text{(from [1, eq. A1])} \\
\dot{x}_5 &= x_6 && \text{(trivial)} \\
\dot{x}_6 &= \frac{1}{I_z - \frac{I_{xz,s}^2}{I_{\phi,s}}} \left(\sum N + \frac{I_{xz,s}}{I_{\phi,s}} \sum L_s \right) && \text{(see below)}
\end{aligned}$$

Derivation of \dot{x}_6 :

$$I_z \dot{x}_6 - I_{xz,s} \dot{x}_8 = \sum N \quad \text{(from [1, eq. A2])} \quad (10)$$

$$I_{\phi,s} \dot{x}_8 - I_{xz,s} \dot{x}_6 = \sum L_s \quad \text{(from [1, eq. A4])} \quad (11)$$

Multiplying (11) with $\frac{I_{xz,s}}{I_{\phi,s}}$ and adding the result to (10) yields

$$\left(I_z - \frac{I_{xz,s}^2}{I_{\phi,s}} \right) \dot{x}_6 = \sum N + \frac{I_{xz,s}}{I_{\phi,s}} \sum L_s$$

Remaining sprung mass dynamics

$$\begin{aligned}
\dot{x}_7 &= x_8 && \text{(trivial)} \\
\dot{x}_8 &= \frac{1}{(I_{\phi,s} - \frac{I_{xz,s}^2}{I_z})} \left(\frac{I_{xz,s}}{I_z} \sum N + \sum L \right) && \text{(see below)} \\
\dot{x}_9 &= x_{10} && \text{(trivial)} \\
\dot{x}_{10} &= \frac{\sum M_s}{I_{y,s}} && \text{(from [1, eq. A6])} \\
\dot{x}_{11} &= \frac{1}{m_s} \sum Y_s - x_6 x_4 && \text{(see below)} \\
\dot{x}_{12} &= x_{13} && \text{(trivial)} \\
\dot{x}_{13} &= g - \frac{1}{m_s} \sum Z_s && \text{(from [1, eq. A5])}
\end{aligned}$$

Derivation of \dot{x}_8 :

Multiplying (10) with $\frac{I_{xz,s}}{I_z}$ and adding the result to (11) yields

$$\left(I_{\phi,s} - \frac{I_{xz,s}^2}{I_z} \right) \dot{x}_8 = \frac{I_{xz,s}}{I_z} \sum N + \sum L_s$$

Derivation of \dot{x}_{11} : Using $a_y = \dot{x}_{11} + x_6 x_4$ from [1, eq. A46] and inserting it in [1, eq. A3] results in

$$m_s(\dot{x}_{11} + x_6 x_4) = \sum Y_s \quad (12)$$

Unsprung mass dynamics (front)

$$\begin{aligned}
\dot{x}_{14} &= x_{15} && \text{(trivial)} \\
\dot{x}_{15} &= \frac{\sum L_{uf}}{I_{u,f}} && \text{(from [1, eq. A17])} \\
\dot{x}_{16} &= \frac{\sum Y_{uf}}{m_{u,f}} - x_6 x_4 && \text{(from (12) and [1, eq. A19])} \\
\dot{x}_{17} &= x_{18} && \text{(trivial)} \\
\dot{x}_{18} &= g - \frac{\sum Z_{uf}}{m_{u,f}} && \text{(from [1, eq. A18])}
\end{aligned}$$

Unsprung mass dynamics (rear)

$$\begin{aligned}
\dot{x}_{19} &= x_{20} && \text{(trivial)} \\
\dot{x}_{20} &= \frac{\sum L_{ur}}{I_{u,r}} && \text{(from [1, eq. A17])} \\
\dot{x}_{21} &= \frac{\sum Y_{ur}}{m_{u,r}} - x_6 x_4 && \text{(from (12) and [1, eq. A19])} \\
\dot{x}_{22} &= x_{23} && \text{(trivial)} \\
\dot{x}_{23} &= g - \frac{\sum Z_{ur}}{m_{u,r}} && \text{(from [1, eq. A18])}
\end{aligned}$$

Convert acceleration input to brake and engine torque This is an addition to [1, Appendix A], which does not explicitly create a positive engine torque if the acceleration demand is positive and a braking torque if the acceleration demand is negative:

$$\begin{aligned}
T_B &= \begin{cases} 0, & \text{for } u_2 > 0 \\ m R_w u_2, & \text{otherwise} \end{cases} \\
T_E &= \begin{cases} m R_w u_2, & \text{for } u_2 > 0 \\ 0, & \text{otherwise} \end{cases}
\end{aligned}$$

Wheel dynamics It is assumed that the brake torque T_B in [1, eq. A55] is split between the front and rear axle according to the newly introduced parameter $T_{s,b}$ (torque split, brake) and the engine torque T_E in [1, eq. A55] is split between the front and rear axle according to the newly introduced parameter $T_{s,e}$ (torque split, engine)

$$\begin{aligned}
\dot{x}_{24} &= \frac{1}{I_{y,w}} (-R_w F_{x,LF} + \frac{1}{2} T_{s,b} T_B + \frac{1}{2} T_{s,e} T_E) && \text{(based on [1, eq. A55])} \\
\dot{x}_{25} &= \frac{1}{I_{y,w}} (-R_w F_{x,RF} + \frac{1}{2} T_{s,b} T_B + \frac{1}{2} T_{s,e} T_E) && \text{(based on [1, eq. A55])} \\
\dot{x}_{26} &= \frac{1}{I_{y,w}} (-R_w F_{x,LR} + \frac{1}{2} (1 - T_{s,b}) T_B + \frac{1}{2} (1 - T_{s,e}) T_E) && \text{(based on [1, eq. A55])} \\
\dot{x}_{27} &= \frac{1}{I_{y,w}} (-R_w F_{x,RR} + \frac{1}{2} (1 - T_{s,b}) T_B + \frac{1}{2} (1 - T_{s,e}) T_E) && \text{(based on [1, eq. A55])}
\end{aligned}$$

Negative wheel spin forbidden This is an addition to [1, Appendix A], which forbids wheel spin in negative direction. When using brake torque, the wheels stay at rest when not moving anymore instead of accelerating in negative direction:

$$\forall i \in \{24, \dots, 27\} : \quad \dot{x}_i = 0 \text{ for } x_i < 0, \quad x_i := 0 \text{ for } x_i < 0$$

Compliant joint equations

$$\dot{x}_{28} = \Delta \dot{y}_F \tag{trivial}$$

$$\dot{x}_{29} = \Delta \dot{y}_R \tag{trivial}$$

5.5 Parameters

The multi-body model requires in total 69 parameters, of which 37 specify the vehicle and 32 the tires. The vehicle parameters of the multi-body model can be found in Tab. 4 and the ones for the tire model in Tab. 5. Please note that in the first version of this document we only consider one parameterization for the tires.

6 Conversion of Initial States and Parameters

As previously mentioned, we do not only like to provide different vehicle models of increasing complexity, but also would like to make results easily comparable. For this reason, we try to specify as many parameters sets for the complicated multi-body model and convert them to simpler models. Similarly, we convert initial states across different models so that results can be compared in the best possible way. We start with converting parameters and afterwards discuss how initial states can be shared across models.

6.1 Conversion of Parameters

From multi-body model to single-track model The single-track model only requires 7 parameters, see Tab. 3. Out of those parameters, 6 parameters are identical to the multi-body model and do not require any conversion:

- total vehicle mass m ,
- moment of inertia for entire mass about z axis I_z ,
- distance from center of gravity to front axle l_f ,
- distance from center of gravity to rear axle l_r ,
- height of center of gravity above ground h_{cg} ,
- friction coefficient μ , which is represented by the parameter p_{Dy1} in [8, Sec. PAC2002].

Only the cornering stiffness coefficient has to be computed: As stated in Sec. 4, we separate the effect of the friction coefficient μ , the cornering stiffness coefficient C_S , and the vertical force F_z , such that the cornering stiffness becomes $C_i = \mu C_{S,i} F_{z,i}$ and $i = \{f, r\}$ for the front and rear axle. The cornering stiffness C_i is by definition the linear approximation of the lateral tire

Table 4: Vehicle Parameters for the multi-body model (see [1, Table E-5.]; values have been converted to SI units). Abbreviations: center of gravity (c.g.), moment of inertia (m.o.i.), suspension (susp.), auxiliary (aux.), damping (damp.).

vehicle parameter			vehicle identifier		
name	symbol	unit	1	2	3
vehicle length	l	[m]	4.298	4.508	4.569
vehicle width	w	[m]	1.674	1.610	1.844
total vehicle mass	m	10^3 [kg]	1.225	1.093	1.478
sprung mass	m_s	10^3 [kg]	1.094	0.965	1.316
unsprung mass (front)	$m_{u,f}$	[kg]	65.67	63.79	81.14
unsprung mass (rear)	$m_{u,r}$	[kg]	65.67	63.79	81.14
distance from c.g. to front axle	l_f	[m]	0.883	1.156	1.150
distance from c.g. to rear axle	l_r	[m]	1.508	1.422	1.321
m.o.i. for m_s in roll	$I_{\phi,s}$	[kg m ²]	244.0	207.2	479.8
m.o.i. for sprung mass about y axis	$I_{y,s}$	10^3 [kg m ²]	1.342	1.565	2.204
m.o.i. for entire mass about z axis	I_z	10^3 [kg m ²]	1.538	1.791	2.473
cross product of inertia for m_s (x-z axis)	$I_{xz,s}$	[kg m ²]	0	0	0
susp. spring rate at each wheel (front)	$K_{S,F}$	10^4 [N/m]	2.189	2.445	3.357
susp. damping rate at each wheel (front)	$K_{SD,F}$	10^3 [N/m]	1.459	1.786	2.405
susp. spring rate at each wheel (rear)	$K_{S,R}$	10^4 [N/m]	2.189	1.963	3.912
susp. damping rate at each wheel (rear)	$K_{SD,R}$	10^3 [N/m]	1.459	1.649	2.769
track width (front)	T_f	[m]	1.389	1.386	1.574
track width (rear)	T_r	[m]	1.423	1.364	1.543
lateral spring rate at compliant pin joint	K_{RAS}	10^5 [N/m]	1.751	1.751	1.751
aux. torsional roll stiffness per axle (front)	$K_{TS,F}$	10^4 [Nm/rad]	-1.28	-0.69	-3.39
aux. torsional roll stiffness per axle (rear)	$K_{TS,R}$	10^3 [Nm/rad]	0	-2.643	-7.731
damp. rate at pin joint btw. m_s and m_u	K_{RAD}	10^4 [Ns/m]	1.021	1.021	1.021
vertical spring rate of tire	K_{ZT}	10^5 [N/m]	1.897	1.582	2.126
c.g. height of total mass	h_{cg}	[m]	0.557	0.574	0.747
height of roll axis above ground (front)	$h_{RA,F}$	[m]	0	0	0
height of roll axis above ground (rear)	$h_{RA,R}$	[m]	0	0	0
m_s c.g. height above ground	h_s	[m]	0.594	0.613	0.804
m.o.i. for $m_{u,f}$ about x-axis (front)	$I_{u,f}$	[kg m ²]	32.53	30.67	50.27
m.o.i. for $m_{u,r}$ about x-axis (rear)	$I_{u,r}$	[kg m ²]	32.53	29.67	48.34
wheel inertia	$I_{y,w}$	[kg m ²]	1.700	1.700	1.700
lateral compliance rate of tire, wheel, susp.	K_{LT}	10^{-5} [m/N]	1.027	1.643	1.223
effective tire radius (RR from [8, PAC2002])	R_w	[m]	0.344	0.344	0.344
torque split of brakes	$T_{s,b}$	[-]	0.76	0.66	0.64
torque split of engine	$T_{s,e}$	[-]	1	0	0
suspension parameter (front)	D_f	[rad/m]	-0.62	-0.39	0
suspension parameter (rear)	D_r	[rad/m]	-0.21	-0.90	0
suspension parameter (front)	E_f	[rad/m ²]	0	0	0
suspension parameter (rear)	E_r	[rad/m ²]	0	0	0

forces. By linearizing the magic tire formula in (9) at zero slip angle, one obtains the following value for the cornering stiffness:

$$C_i = B_y C_y D_y = \frac{K_{y,i}}{C_y D_{y,i}} C_y D_y = K_{y,i} = F_{z,i} p_{Ky1}$$

so that

$$C_{S,i} = \frac{p_{Ky1}}{\mu} = \frac{p_{Ky1}}{p_{Dy1}}.$$

Table 5: Tire Parameters (see [8, Sec. PAC2002]).

name	symbol	value
longitudinal parameters		
shape factor for longitudinal force	p_{Cx1}	1.6411
longitudinal friction μ_x at F_{z0}	p_{Dx1}	1.1739
variation of friction μ_x with camber	p_{Dx3}	0
longitudinal curvature at F_{z0}	p_{Ex1}	0.4640
longitudinal slip stiffness at F_{z0}	p_{Kx1}	22.303
horizontal shift at F_{z0}	p_{Hx1}	$1.2297 \cdot 10^{-3}$
vertical shift at F_{z0}	p_{Vx1}	$-8.8098 \cdot 10^{-6}$
slope factor for combined slip F_x reduction	r_{Bx1}	13.276
variation of slope F_x reduction with κ	r_{Bx2}	-13.778
shape factor for combined slip F_x reduction	r_{Cx1}	1.2568
curvature factor of combined F_x	r_{Ex1}	0.6522
shift factor for combined slip F_x reduction	r_{Hx1}	$5.0722 \cdot 10^{-3}$
lateral parameters		
shape factor for lateral forces	p_{Cy1}	1.3507
lateral friction μ_y	p_{Dy1}	1.0489
variation of friction μ_y with squared camber	p_{Dy3}	-2.8821
lateral curvature at F_{z0}	p_{Ey1}	$-7.4722 \cdot 10^{-3}$
maximum value of stiffness	p_{Ky1}	-21.920
horizontal shift at F_{z0}	p_{Hy1}	$2.6747 \cdot 10^{-3}$
variation of shift with camber	p_{Hy3}	$3.1415 \cdot 10^{-2}$
vertical shift at F_{z0}	p_{Vy1}	$3.7318 \cdot 10^{-2}$
variation of vertical shift with camber	p_{Vy3}	-0.3293
slope factor for combined F_y reduction	r_{By1}	7.1433
variation of slope F_y reduction with α	r_{By2}	9.1916
shift term for α in slope F_y reduction	r_{By3}	$-2.7856 \cdot 10^{-2}$
shape factor for combined F_y reduction	r_{Cy1}	1.0719
curvature factor of combined F_y	r_{Ey1}	-0.2757
shift factor for combined F_y reduction	r_{Hy1}	$5.7448 \cdot 10^{-6}$
κ -induced side force at F_{z0}	r_{Vy1}	$-2.7825 \cdot 10^{-2}$
variation of $S_{Vy\kappa}/\mu_y F_z$ with camber	r_{Vy3}	-0.2756
variation of $S_{Vy\kappa}/\mu_y F_z$ with α	r_{Vy4}	12.120
variation of $S_{Vy\kappa}/\mu_y F_z$ with κ	r_{Vy5}	1.9
variation of $S_{Vy\kappa}/\mu_y F_z$ with $\arctan(\kappa)$	r_{Vy6}	-10.704

From single-track model to kinematic single-track model This conversion is trivial: We only require the wheelbase $l_{wb} = l_f + l_r$.

6.2 Conversion of Initial States

We like to initialize all models such that their initial behavior is simliar. However, it is possible to initialize the model differently, but then this different initialization has to be explicitly stated. In order to facilitate switching between different models, we share the following initial values across all models:

- initial x-position $s_{x,0}$,
- initial y-position $s_{y,0}$,
- initial velocity v_0 ,
- initial orientation Ψ_0 ,
- initial yaw rate $\dot{\Psi}_0$,

- initial slip angle β_0 .

Multi-body model Since the multi-body model is tedious to initialize, we propose an initialization using the following auxiliary values:

- $\omega_0 = \frac{v_{x,0}}{R}$ (no wheel spin, R : effective tire radius),
- $v_{x,0} = \cos(-\beta_0)v_0$ (velocity in longitudinal direction from slip angle β),
- $v_{y,0} = \sin(-\beta_0)v_0$ (velocity in lateral direction from slip angle β),
- $v_{yf,0} = v_{y,0} + l_f \dot{\Psi}_0$ (lateral velocity at front axle from velocity at c.g. and yaw rate),
- $v_{yr,0} = v_{y,0} - l_r \dot{\Psi}_0$ (lateral velocity at rear axle from velocity at c.g. and yaw rate),
- $z_{i,0} = \frac{F_{zi,0}}{2K_{zt}}$ ($i \in \{r, f\}$) (height over ground so that springs support weight),
- $\delta_0 = \frac{v_0(l_f + l_r)}{C_{S,f} g l_r \mu} \dot{\Psi}_0 + \frac{1}{C_{S,f} l_r} ((C_{S,r} l_f + C_{S,f} l_r) \beta_0 - (C_{S,r} - C_{S,f}) l_r l_f \frac{\dot{\Psi}_0}{v_0})$ (initial steering angle from steady state of slip angle).

The initial steering angle is derived from demanding that the slip angle β of the single-track model is at steady state for $a_{\text{long}} = 0$ (see (8)):

$$\frac{x_4(l_r + l_f)}{C_{S,f} g l_r \mu} x_6 + \frac{1}{C_{S,f} l_r} \left((C_{S,r} l_f + C_{S,f} l_r) x_7 - (C_{S,r} - C_{S,f}) \frac{l_f l_r x_6}{x_4} \right) = x_3.$$

Inserting these values in Tab. 6 initializes the multi-body model as proposed in this document.

Table 6: Initial values of the multi-body model.

sprung mass			unsprung mass			other		
name	symp.	init. val.	name	symp.	init. val.	name	symp.	init. val.
yaw ang.	$x_{5,0}$	Ψ_0	roll ang. (f)	$x_{14,0}$	0	wheel speed (LF)	$x_{24,0}$	ω_0
yaw rate	$x_{6,0}$	$\dot{\Psi}_0$	roll rate (f)	$x_{15,0}$	0	wheel speed (RF)	$x_{25,0}$	ω_0
roll angle	$x_{7,0}$	0	roll ang. (r)	$x_{19,0}$	0	wheel speed (LR)	$x_{26,0}$	ω_0
roll rate	$x_{8,0}$	0	roll rate (r)	$x_{20,0}$	0	wheel speed (RR)	$x_{27,0}$	ω_0
pitch ang.	$x_{9,0}$	0	y-vel. (f)	$x_{16,0}$	$v_{yf,0}$	pin joint diff. (f)	$x_{28,0}$	0
pitch rate	$x_{10,0}$	0	y-vel. (r)	$x_{21,0}$	$v_{yr,0}$	pin joint diff. (r)	$x_{29,0}$	0
x-velocity	$x_{4,0}$	$v_{x,0}$	z-pos. (f)	$x_{17,0}$	$z_{f,0}$	x-position	$x_{1,0}$	$s_{x,0}$
y-velocity	$x_{11,0}$	$v_{y,0}$	z-vel. (f)	$x_{18,0}$	0	y-position	$x_{2,0}$	$s_{y,0}$
z-position	$x_{12,0}$	0	z-pos. (r)	$x_{22,0}$	$z_{r,0}$	steering angle	$x_{3,0}$	δ_0
z-velocity	$x_{13,0}$	0	z-vel. (r)	$x_{23,0}$	0			

Single-track model The initialization of the single-track model is straightforward:

$$x_{1,0} = s_{x,0}, \quad x_{2,0} = s_{y,0}, \quad x_{3,0} = \delta_0, \quad x_{4,0} = v_0, \quad x_{5,0} = \Psi_0, \quad x_{6,0} = \dot{\Psi}_0, \quad x_{7,0} = \beta_0.$$

Kinematic single-track model Similarly, the initialization of the kinematic single-track model is straightforward:

$$x_{1,0} = s_{x,0}, \quad x_{2,0} = s_{y,0}, \quad x_{3,0} = \delta_0, \quad x_{4,0} = v_0, \quad x_{5,0} = \Psi_0.$$

Point-mass model The initialization of the point-mass model only requires initial positions and velocities:

$$x_{1,0} = s_{x,0}, \quad x_{2,0} = s_{y,0}, \quad x_{3,0} = v_0 \cos(\Psi_0), \quad x_{4,0} = v_0 \sin(\Psi_0).$$

7 Examples

In this section, we perform numerical experiments based on the parameters of vehicle 2 (BMW 320i): First, we compare the kinematic single-track model, the single-track model and the multi-body model in a left curve. Secod, we demonstrate understeering and oversteering for the multi-body model during cornering. For all experiments we use the following initial states:

$$s_{x,0} = s_{y,0} = \Psi_0 = \dot{\Psi}_0 = \beta_0 = 0, \quad v_0 = 15.$$

The simulation time for all tests is 1 s.

Comparison of KS, ST and MB during cornering We perform a left curve by choosing $v_\delta = 0.15$ [rad/s]. Fig. 2(a) shows the paths of the kinematic single-track model, the single-track model and the multi-body model. It can be easily seen that the kinematic single-track model realizes the tightest bend since it does not consider tire slip; the single-track model is a little wider due to considering tire slip. This effect is even stronger for the multi-body model since its vehicle model considers saturation of tire forces. This can be even better seen when comparing the slip angles of the single-track model and the multi-body model in Fig. 2(b).

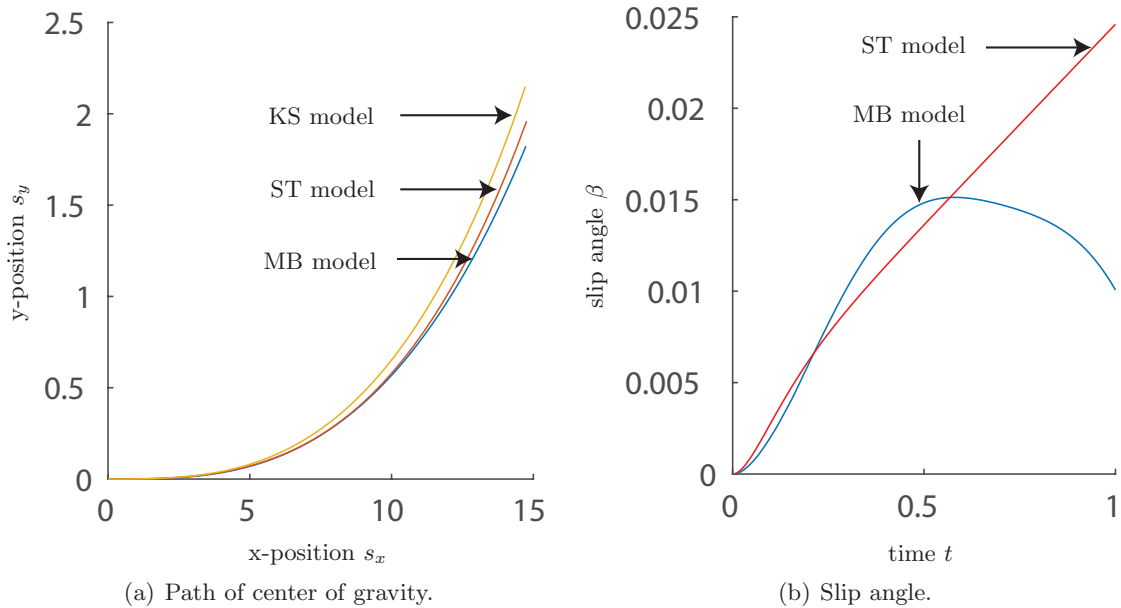


Figure 2: Comparing the kinematic single-track (KS) model, the single-track (ST) model and the multi-body (MB) model during cornering.

Oversteering and understeering of the multi-body model During cornering, a vehicle tends to understeer when braking since typically more braking force is applied at the front brakes: Oversteering during braking would make a vehicle much less safe to drive. Oversteering can be achieved by accelerating with a rear-wheel-drive vehicle during cornering. Fig. 3(a) shows the paths of the multi-body model when using again $v_\delta = 0.15$ [rad/s] and in addition

$a_{\text{long}} = -0.7 \text{ g}$ for braking and $a_{\text{long}} = 0.63 \text{ g}$ for acceleration. The tightest bend is realized by braking since the velocity drops and the widest bend is caused by accelerating since the velocity increases. It is evident that during braking we have understeer and during acceleration we have oversteer by observing the slip angle in Fig. 3(b). This is also obvious from the orientation of the vehicle, where during acceleration, the vehicle turns into the corner as shown in Fig. 3(c). Further, in Fig. 3(d) the pitch for braking shows that the vehicle is “diving” while the front lifts during acceleration. This plot also nicely shows the oscillation in the spring-mass-damper system since braking and acceleration is suddenly applied.

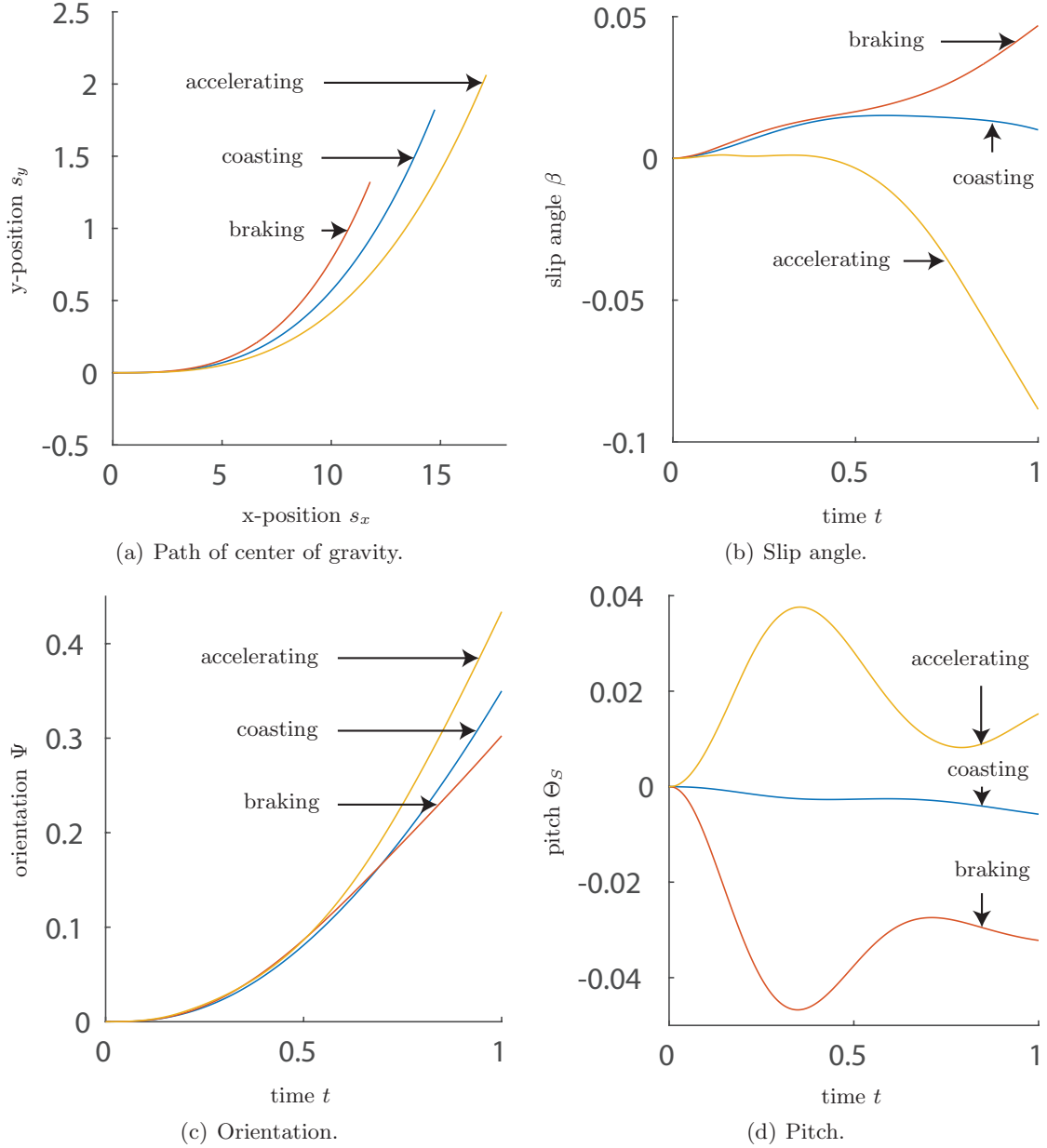


Figure 3: Investigating oversteering and understeering for the multi-body model.

8 Conclusions

This document describes four models for motion planning of automated vehicles as part of the *CommonRoad* benchmark suite: point-mass model, kinematic single-track model, single-track

model, and a multi-body model. To easily exchange models, we also present how to convert parameters and initial states from the multi-body model to simpler models. The sources of all equations are carefully referenced in this work and all models are available as MATLAB and Python code. Numerical experiments provide further insight into what effects certain models can show.

Acknowledgment

The author gratefully acknowledge financial support by the Free State of Bavaria.

References

- [1] R. W. Allen, H. T. Szostak, D. H. Klyde, T. J. Rosenthal, and K. J. Owens. Vehicle dynamic stability and rollover. Final Report DOT HS 807 956, U.S. Department of Transportation, 1992.
- [2] M. Althoff and S. Magdici. Set-based prediction of traffic participants on arbitrary road networks. *IEEE Transactions on Intelligent Vehicles*, 1(2):187–202, 2016.
- [3] E. Bertolazzi, F. Biral, and M. Da Lio. Real-time motion planning for multibody systems. *Multibody System Dynamics*, 17(2):119–139, 2007.
- [4] P. Gaspar, I. Szaszi, and J. Bokor. Reconfigurable control structure to prevent the rollover of heavy vehicles. *Control Engineering Practice*, 13:699–711, 2005.
- [5] D. N. Godbole, V. Hagenmeyer, R. Sengupta, and D. Swaroop. Design of emergency maneuvers for automated highway system: Obstacle avoidance problem. In *Proc. of the 36th Conference on Decision & Control*, pages 4774–4779, 1997.
- [6] J. H. Jeon, S. Karaman, and E. Frazzoli. Anytime computation of time-optimal off-road vehicle maneuvers using the rrt*. In *Proc. of the 50th IEEE Conference on Decision and Control and European Control Conference*, pages 3276–3282, 2011.
- [7] D. Kim, H. Peng, S. Bai, and J. M. Maguire. Control of integrated powertrain with electronic throttle and automatic transmission. *IEEE Transactions on Control Systems Technology*, 15(3):474–482, 2007.
- [8] MSC Software, 2 MacArthur Place, Santa Ana, CA 92707. *Adams/Tire help*, April 2011. Documentation ID: DOC9805.
- [9] D. Odenthal, T. Bünte, and J. Ackermann. Nonlinear steering and braking control for vehicle rollover avoidance. In *Proc. of the European Control Conference*, pages 598–603, 1999.
- [10] H. B. Pacejka. *Tyre and Vehicle Dynamics*. Butterworth-Heinemann, 2002.
- [11] B. Paden, M. Čáp, S. Z. Yong, D. Yershov, and E. Frazzoli. A survey of motion planning and control techniques for self-driving urban vehicles. *IEEE Transactions on Intelligent Vehicles*, 1(1):33–55, 2016.
- [12] S. Petti and Th. Fraichard. Safe motion planning in dynamic environments. In *Proc. of the Conference on Intelligent Robots and Systems*, 2005.
- [13] R. Rajamani. *Vehicle Dynamics and Control*. Springer, 2012.

- [14] Z. Shiller and Y.-R. Gwo. Dynamic motion planning of autonomous vehicles. *IEEE Transactions on Robotics and Automation*, 7(2):241 – 249, 1991.
- [15] S. E. Shladover, C. A. Desoer, J. K. Hedrick, M. Tomizuka, J. Walrand, W.-B. Zhang, D. H. McMahon, H. Peng, S. Sheikholeslam, and N. McKeown. Automated vehicle control developments in the PATH program. *IEEE Transactions on Vehicular Technology*, 40(1):114–130, 1991.
- [16] J.-B. Tomas-Gabarron, E. Egea-Lopez, and J. Garcia-Haro. Vehicular trajectory optimization for cooperative collision avoidance at high speeds. *IEEE Transactions on Intelligent Transportation Systems*, 14(4):1930–1941, 2013.